Materials Research Express

PAPER • **OPEN ACCESS**

Site-substitution effect on skyrmion phases of Cd^{2+}-Cu_2OSeO_3 nanocrystallites

To cite this article: S Babu *et al* 2020 *Mater. Res. Express* **7** 105002

Materials Research Express

PAPER

Site-substitution effect on skyrmion phases of Cd^{2+}-Cu_2OSeO_3 nanocrystallites

S Babu, B K Singh and S K Mishra

School of Materials Science and Technology, Indian Institute of Technology (BHU), Varanasi-221 005, India

E-mail: shrawan.mst@iitbhu.ac.in

Keywords: noncollinear magnetism, nanomagnetism, spin helix, nanomaterials

OPEN ACCESS

RECEIVED
24 June 2020

REVISED
17 September 2020

ACCEPTED FOR PUBLICATION
23 September 2020

PUBLISHED
7 October 2020

Abstract

The past decade has seen a significant uptick in research interest to study the materials that can host magnetic skyrmion lattices. The curiosity of such materials is mainly driven by the technological applications of emergent skyrmion lattices that manifest a whirlpool-like spins arrangement. Insulating Cu_2OSeO_3 reported to host magnetic skyrmion lattices below 60 K and considered as a potential candidate for exploring this new phase of materials. Here in this article, we propose a new synthesis process to grow the Cd^{2+}-substituted Cu_2OSeO_3 nanocrystallites with variable sizes ranging over 50–200 nm. The proposed method consists of only a single-step heat treatment of 12 h, which is cost-effectivethan the routine solid-state process that requires a rigorous 15–20 days of heat treatment. By employing X-ray diffraction (XRD), transmission electron microscopy (TEM), energy dispersive X-ray analysis (EDX), X-ray photoelectron spectroscopy (XPS), and isothermal magnetization (M-T) measurements, we present a comparative investigation of the structural, electronic and magnetic properties of pristine and Cd^{2+}-substituted Cu_2OSeO_3 nanocrystallites. As non-magnetic substitution can alter the fundamental magnetic interactions, therefore, Cd^{2+}-Cu_2OSeO_3 nanocrystallites offer a new methodology to control the magnetic skyrmion phases and its stability.

1. Introduction

The magnetic skyrmion lattices are a new state of matter with swirling spin, which protected from external perturbation through an intrinsic topological potential barrier [1]. This prevents skyrmion lattices from thermal fluctuation so that spin structure can remain intact. The energy barrier that established from the discontinuity to transmute between spin structures with topological charges *n*, which count the spin swirl around a unit sphere. $n = 1$ results in the skyrmion lattice and $n = 0$ results in the other non-collinear spin structure such as conical, spin helix and other complex collinear spin states orderings [1–3]. The discovery has mainly driven by the extensive investigation of skyrmion since they proposed to drive by ultra-low spin polarized current [4], turning magnetic skyrmion as a potential candidate for energy efficient magnetic memory and other spintronic devices.

For a chiral spin system, the broken inversion symmetry stabilizes an asymmetric exchange interaction (Dzyaloshinskii-Moriya (DM)) that enforces a canted arrangement to the adjacent neighbouring spins [3, 5–7]. These competing interactions results a non-colinear spin arrangement that responsible for stabilizing the trivial spin systems such as cycloid and helical spin orderings.

In a skyrmion lattice, the competition between the exchange interaction (J) and the asymmetric DM interaction (D) is a key factor that governs the formation and stablization of skyrmion lattices. The local exchange energy $E_{i;j}$ for such system is expressed as $E_{i;j} = -J(S_i.S_j) + D(S_i.S_j)$, where S_i and S_j are the neighbouring spin sites, and $D = |D|$. The length scale of an isolated stable skyrmion is estimated by ratio (J/D). a_{mag}, where a_{mag} is the magnetic lattice periodicity [8]. The stability of the skyrmion relies on the size of the skyrmion and the system size (L). For a chiral spin system, the skyrmion lattices are stabilized in the absence of an external magnetic field for $L > (J/D).\ a_{mag}$. However, for $(J/D).\ a_{mag} = L$, the ground state could be degenerate with ferrimagnetic state and/or skyrmionics state [9]. In the presence of any thermal perturbation, a critical

values of magnetic anisotropies magnetic frustration, the magnetic skyrmion lattice is energetically favoured and a skyrmion phase in a plane perpendicular to the direction of an applied magnetic field can develop [10].

The skyrmion phase has been manifested in the intermetallic alloy Co-Zn-Mn [11, 12], thin film and bulk MnSi [13, 14], and bulk Cu_2OSeO_3 [15, 16] that offer unique opportunity to extend the investigation of these materials. One popular strategy to discover new helical spin system is redefining the non-centrosymmetric crystal lattices that have been well-known skyrmion host systems. Even after a decade of intensive investigations, skyrmion-hosting materials remain notable small in number. Specific structural properties such as the lack of inversion symmetry and magnetic features like ferromagnetism and the presence of DM interactions is essential to establish the evolution of magnetic skyrmion [1–3]. The popular means to enhance the number of host materials is chemical doping in well-known canonical skyrmion-hosting systems. This method has been already examined for Cu_2OSeO_3 skyrmion lattice by substituting Cu with Zn and Ni that generate significant modifications in intrinsic skyrmion phases [17, 18].

Generally, the Mott insulator Cu_2OSeO_3 crystallizes in non-centrosymmetric $P2_13$ space group. Two Cu^{2+} cations in trigonal bipyramidal (Cu_I) and square pyramidal (Cu_{II}) coordination geometry are present that responsible for forming a ferrimagnetic lattice [19–21]. The magnetic exchange interactions between spins are interlinked by oxygen atoms via super-exchange interactions [22, 23]. It has been reported that magnetic moment of Cu_2OSeO_3 monotonically decreases with increasing Zn-substitution levels [17]. This effect has been interpreted in terms of the site-specific substitution of Cu^{2+} cation at the Cu_{II}-site by a non-magnetic Zn^{2+}. Stefancic *et al* [24] observed splitting of the skyrmion phase in $(Cu_{1-x}Zn_x)_2OSeO_3$ attributed to the multiphase nature of the polycrystalline nature of host materials. Sukhanov *et al* [25] observed that Cu ions are replaced by either magnetic (nonmagnetic) within a critical limit of low impurity concentration in Cu_2OSeO_3 found that all the substituted compounds possess a helical spin structure in applied magnetic fields at temperatures near to T_C which was very identical to the pristine Cu_2OSeO_3 [17, 24, 25].

In this study, we grew and investigated the Cd-doped Cu_2OSeO_3 nanocrystallites as host materials for magnetic skyrmion. The structural, electronic and magnetic properties of both Cd-doped and pristine Cu_2OSeO_3 were investigated. Experimental findings suggest that chemical substitution stabilized the magnetic skyrmion lattices.

2. Experimental methods

Cd-doped Cu_2OSeO_3 crystallites were synthesised by the conventional solid-state reaction. Stoichiometric mixtures of CuO and SeO_2 precursor powders were ground manually and pressed in the form of pallets. The pallets were then sealed in an evacuated quartz tube. The reaction mixture took placed at elevated temperature 600 °C that was ramped up with a constant rate of 50 °C h^{-1} for 12 h. This thermal treatment followed by quenching of reaction tube in a water bath. This reaction results a greenish powder that mostly a mixed-phase compound. To obtain the undoped sample in pure phase, we performed a routine heat-treatment with various intermediate stages for 15 days, as illustrated in figure 1(a), The olive-green colour single-crystalline nanocrystals of the undoped samples were obtained. Interestingly, with nominal Cd-doping followed by one step heat-treatment for 12 h $(Cu_{1-x}Cd_x)_2OSeO_3$ ($x = 0.02$) were obtained. Finally, the resulting a dark greenish single-phase nanocrystal (1(b)). Both doped and pristine samples were used for further various characterizations and analysis.

The crystal structure and phase purity identification of the samples were determined via x-ray diffraction (XRD) using an X-ray diffractometer (Rigaku, Mini Flex 300/600, Japan). Cu-K_α ($\lambda = 1.5406$ A) was used as a probe source. The XRD patterns were refined with the FullProf Suite [26]. For the analysis, the diffraction patterns were recorded in the range of 10–90 degrees with a constant scan rate was 2 degree min^{-1} with a step size of 0.02 degree. Rietveld refinement of XRD patterns was consistent with single-phase cubic Cu_2OSeO_3 ($P2_13$). No other impurities phases were detected within the limit of experimental noise. The observed broad diffracted peaks were indicating the formation of nanosized crystallites of Cu_2OSeO_3. The average crystallite sizes of the samples were estimated using the Scherrer formula [27]. TEM (Tecnai G2 20 TWIN, USA) was used to study the microstructure and crystalline properties. Selected area electron diffraction (SAED) data were indexed by CrysTBox software [28]. Homogeneity and elemental compositions were analysed with the EDX. The oxidation states of the constituent elements and stoichiometry were investigated through X-ray photoelectron spectroscopy (XPS) measurements, which was performed on both doped and pristine samples. The survey XPS maps of Cu-2p, O-1s, and Se-3p were collected using Al-Kα. SQUID-VSM magnetometer (MPMS-3X, Quantum Design) was used to detect the effect of Cd-doping on temperature-dependent magnetic properties (M-T).

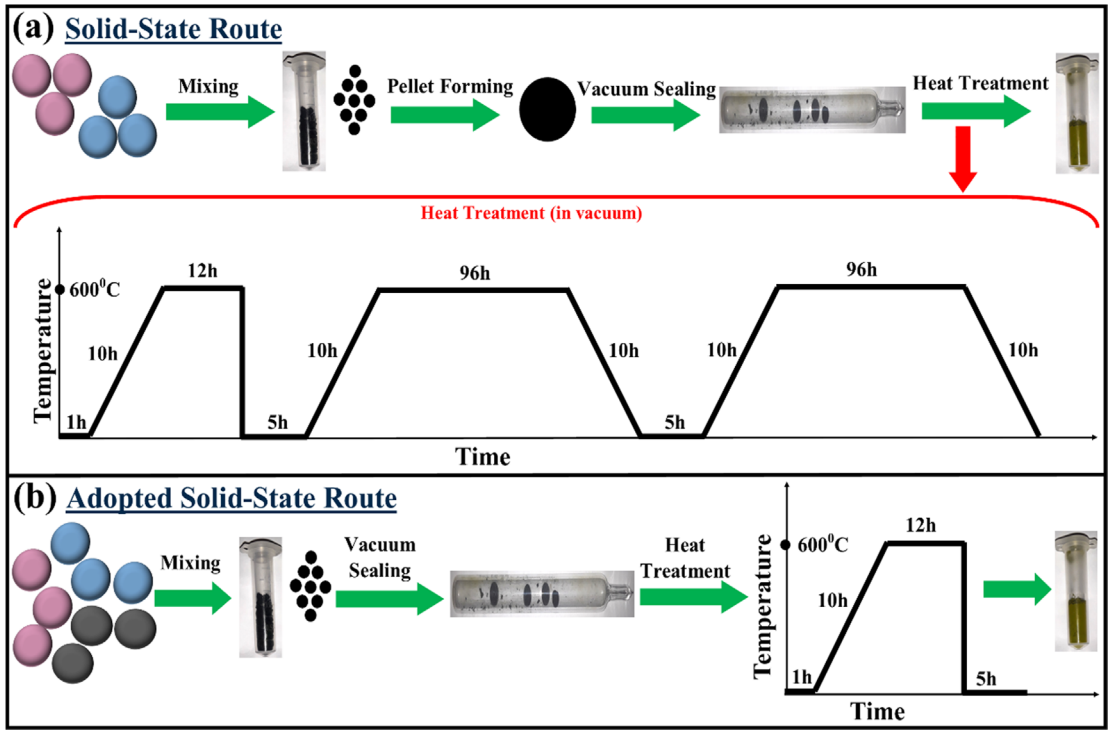

Figure 1. Systematic for the synthesis of Cu_2OSeO3 and $(Cu_{0.98}Cd_{0.02})_2OSeO_3$ nanocrystallites.

3. Results and discussions

Figure 2(a) shows the XRD pattern of pristine and Cd-doped Cu_2OSeO_3 quenched sample at 600 °C represents the mixed-phase. The observed peak positions and diffraction patterns are in well agreement with JCPDS database of Cu_2OSeO_3 powder sample. With rigorous heat-treatment processes of nearly 15 days undoped sample transform into a single phase that suggests a perfect matching with literature single phase as shown in figure 2(a). With nominal doping of Cd (2%) on Cu_2OSeO_3 followed by one step heat-treatment, alternatively, we also grown a single-phase non-crystalline sample. The XRD patterns of the both doped and undoped samples ensured that both of the samples possessing an identical crystal structure as depicted in figure 2(a).

A well indexed XRD patterns along with simulated XRD diffraction patterns are shown in figure 2(b). The background and peak shape fitted with linear interpolation and pseudo-Voigt function using Full Prof Software Suite [26]. Lattice parameters, scale factor, and positional coordinates were varied to obtain the agreement factor with fitted parameters like R_p, R_{wp}, R_e and χ^2 are 18.5, 17.0, 10.6, and 2.55, respectively. Figure 2(b) also depicts a relative comparison between the experimental (open black circles) and simulated (solid red line) XRD patterns, which are in good agreement as can be realized from the difference curve (blue bottom line). Most of the Bragg's reflections (vertical green bar) are in an excellent agreement with experimental patterns. The lattice parameters ($a = b = c = 8.9330(4) A^\circ$, and $\alpha = \beta = \gamma = 90^\circ$) were used in well-matched with single-phase cubic structure having space group $P2_13$ (JCPDS database card No.: 000460793). The crystallite size (D) of both doped and undoped samples was calculated by estimating the full width at half maxima (FWHM) of the prominent and intense XRD peaks and applying the Scherrer formula [27]. The typical obtained value of D was ranging from 45 and 50 nm. Nominal doping of Cd (2%) can enhance the nucleation sites to the lattice system, as confirmed in Figure 2(b). The quenching induces the residual stresses between Cu_2OSeO_3 matrices and the reinforced particles along with strain [29, 30].

Figure 3 shows the TEM images and SAED pattern of $(Cu_{1-x}Cd_x)_2OSeO_3$ ($x = 0.2$) nanocrystals. The elongated crystallites were clearly observed as shown in figure 3(a). The average size of these crystallites range over 50–200 nm. The TEM image of $(Cu_{1-x}Cd_x)_2OSeO_3$ ($x = 0.2$) is depicted in figure 3(b). The lattice fringes indicate a high crystallinity of the Cu_2OSeO_3 nanocrystal with the inter-planar spacing (d) of 0.5035 nm corresponds to (1 1 1) plane. The obtained d value was comparable to estimated data from XRD patterns. Figure 3(c) shows the SAED pattern that verifies the high crystallinity of the nanocrystal. The enlarged view of

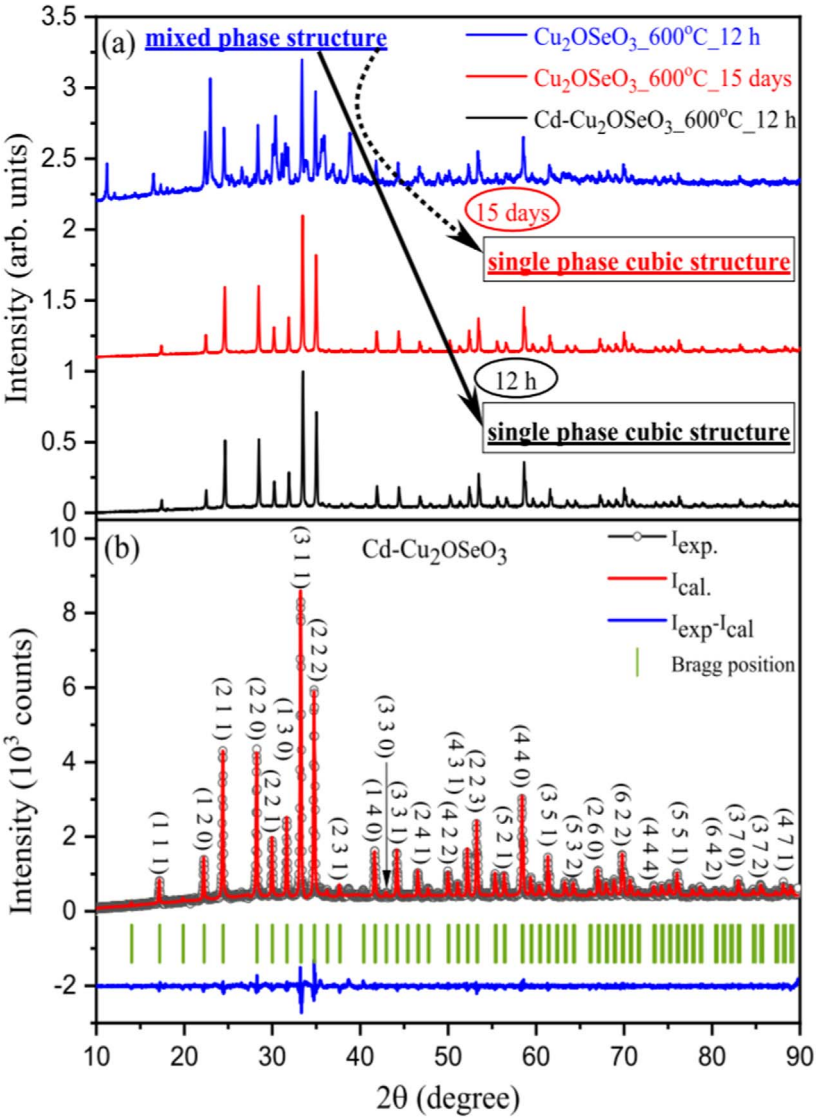

Figure 2. (a) XRD pattern evolution of the $(Cu_{0.98}Cd_{0.02})_2OSeO_3$ powder samples for various stages of heat-treatments from the mixed phase to single phase, and (b) single phase refined XRD pattern for $(Cu_{0.98}Cd_{0.02})_2OSeO_3$ sample.

figure 3(c) shows the well-indexed SAED pattern and further confirmed the cubic crystal structure. The inter-planar spacings estimated from SAED patterns, shows a good agreement with XRD data.

The single-crystalline SAED patterns were reported with experimental results in poly crystalline Cu_2OSeO_3 powders, which is theoretical in well agreement for a cubic system and hold the d (inter-planer spacing) and R (distance between transmitted and diffracted beam) relation for a cubic system, $d_1/d_2 = R_2/R_1 = \sqrt{N_2}/\sqrt{N_1}; N \equiv h^2 + k^2 + l^2$. In consonance with figure 3(d), the angle between the planes $(\bar{1}10)$ and $(\bar{3}03)$, $(\bar{3}03)$ and $(\bar{2}\bar{1}3)$, $(\bar{2}\bar{1}3)$, and $(\bar{1}\bar{2}\,3)$, $(1\bar{1}0)$ are 60.15°, 19.23°, 60.15°, 78.76°, respectively, interpreted with the CrysTBox software [28]. The expression between angle and miller indices for cubic system is can be written as

$$\cos(\theta) = \frac{h_1h_2 + k_1k_2 + l_1l_2}{\sqrt{(h_1^2 + k_1^2 + l_1^2)(h_2^2 + k_2^2 + l_2^2)}} \quad (1)$$

where θ is corresponding angle between $(h1, k1, l1)$ and $(h2, k2, l2)$ crystallographic planes. All angles between the different crystallographic planes measured from SAED pattern are in excellent agreement with angles estimated from equation (1). The crystallographic zone axis is estimated to be [111] that indicates single-crystalline cubic Cu_2OSeO_3 nanocrystals growth direction and all indexed planes are correspond to the zone axis. The elemental mapping and EDX spectra of Cd-doped Cu_2OSeO_3 are shown in figure 4. The scanned image of sample $(Cu_{0.98}Cd_{0.02})_2OSeO_3$ is shown in figure 4(a), and complete elemental scan of Cu-K, Cd-L, Se-K and O-K shown in figure 4(b). Individual mapping of elements (Cu, Cd, Se, and O) present in $(Cu_{0.98}Cd_{0.02})_2OSeO_3$

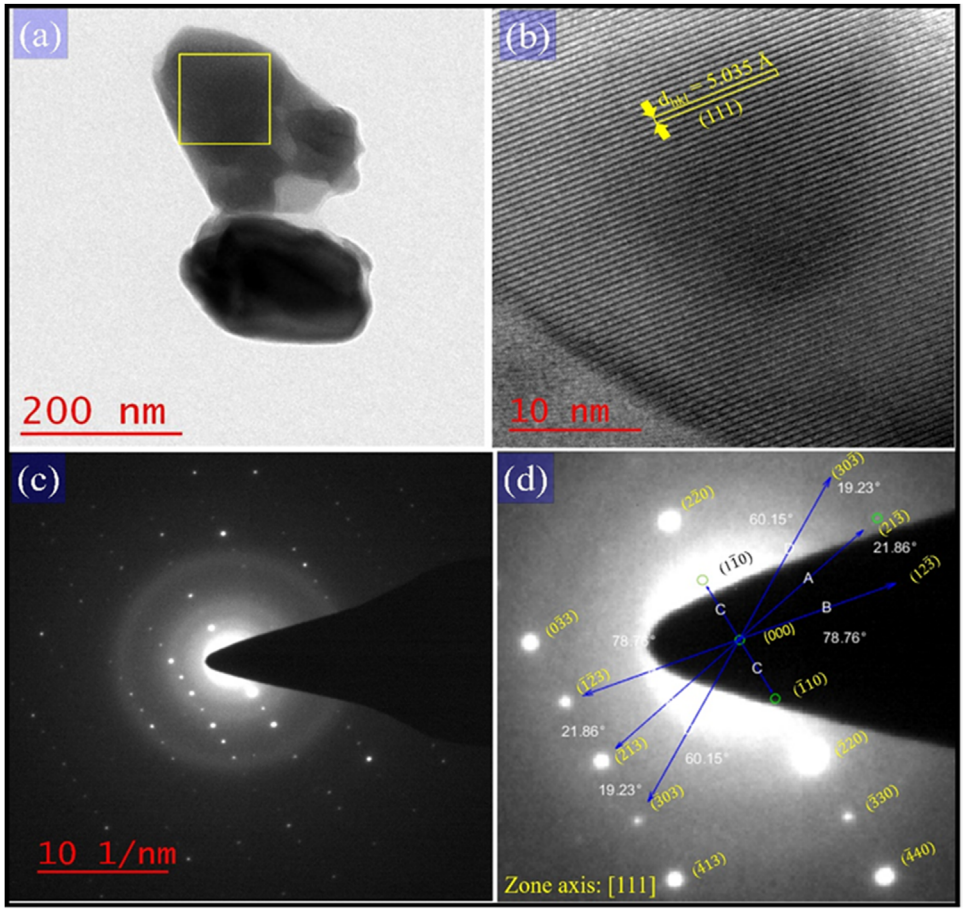

Figure 3. (a) TEM image of Cd-substituted Cu_2OSeO_3 nanocrystals prepared by adopted solid-state route, HRTEM image (b) of individual Cd-substituted Cu_2OSeO_3 nanocrystals, and the corresponding SAED pattern (c) and enlarge and indexed pattern (d).

are distributed uniformly throughout the nanocrystallites as shown in figures 4(c)–(f). EDS spectra for the present elements like Cu, Cd, O, and Se represent the atomic fraction of elements (see figure 4(g)), which is in well agreement to that the doped Cu_2OSeO_3 revealing the excellent quality of nanocrystallites.

The valence states of the elements were probed by XPS spectra which were performed on the freshly prepared $(Cu_{0.98}Cd_{0.02})_2OSeO_3$. WIDE XPS spectra of Cd-2p, Cu-2p, O-1s and Se-3p were collected using a non-monochromatic Al-K energy (E = 1487.6 eV) X-ray source and an electron-analyser. Figures 5(a)–(g) shows the XPS spectra of nanoparticles corresponding to Cd-2p, Cu-2p, O-1s, and Se-3p. The binding energies (BE) of elements were matched with C-1s (BE = 284.8 eV peak. Cu-2p spectra (figures 5(b)–(c)) deconvoluted into different individual peaks for binding energies of 934.3 eV, 954.1 eV, 943.6 and 962.5 eV. The BE of the Cu-2p core level at 934.3 and 954.1 eV can be attributed to Cu-$2p_{3/2}$ and Cu-$2p_{1/2}$, respectively. Cu-$2p^*_{3/2}$ (BE = 943.5 eV) and Cu$2p^*1/2$ (962.5 eV) are the Cu-satellite peaks.

The Cu-2p satellite peaks are indicating the presence of Cu in 2 + valence state [31]. XPS spectra of O-1s (figures 5(d)–(e)) show peak at 530.7 eV that can be attributed to bulk O2− of the cubic lattice system. Experimental data suggest an absence of any chemisorbed oxygen, indicating the excellent stoichiometry of Cu_2OSeO_3 nanoparticles. Figures 5(f)–(g) shows the BE at 164.7 and 170.3 eV that correspond to Se-3p3/2 and Se-3p1/2 orbitals, respectively. These peaks represent the Se 4 + valence state. The relative areas of Se-2p and Cu-2p suggest that Se to Cu atomic ratio of approximately 1:2 and indicate the stoichiometry of Cu_2OSeO_3 nanoparticles. Table (1) shows the details of fitted parameters like BE FWHM, peaks area for both undoped and doped samples.

The temperature-dependent magnetization measurements were conducted in zero field cooled (ZFC) protocol with an applied field of 250 Oe for the doped and pristine samples are shown in figure 6. Curie temperature (T_C = 63.87(22) K) and Curie constant ($C = 2.96 \times 10\text{-}6$) of the quenched sample, which is well consistent with the reported data. For Cd-doped Cu_2OSeO_3, the ferrimagnetic transition temperature is almost insensitive to Cd concentration having a minimal variation in moments for nominal Cd doping.

The inset figure 6(a) shows the ($1/\chi_{dc}$, T) magnetic susceptibility and revealing transition temperature of 63.87(22) K, which is same as reported in the bulk material. This suggests that this material is not only similar to

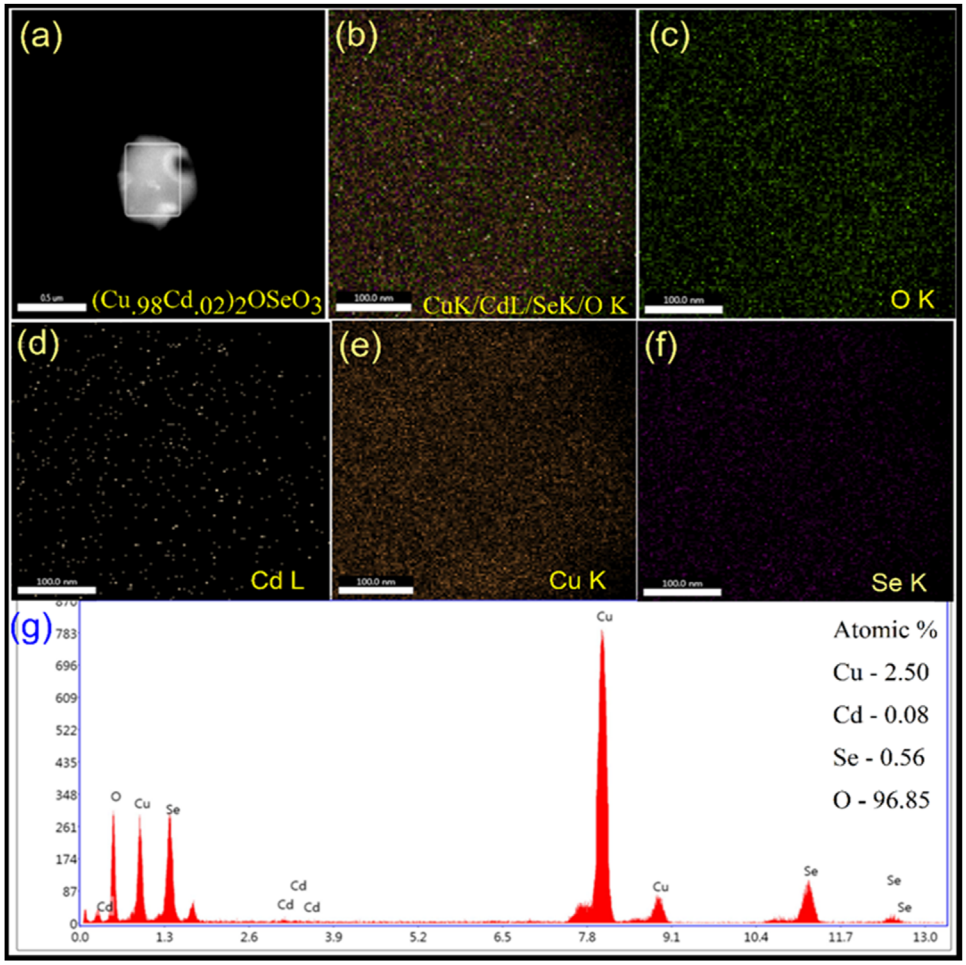

Figure 4. Elemental mapping and EDX data. (a) Image of sample $(Cu_{0.98}Cd_{0.02})_2OSeO_3$ and (b) complete elemental scan of Cu, Cd, Se and O.(c)–(f) Individual mapping of elements present in $(Cu_{0.98}Cd_{0.02})_2OSeO_3$ and (g) EDS spectra for the present elements like Cu, Cd, Se, and O, equipped with transmission electron microscope.

Table 1. Fitting parameters for elements O, Cu, Se and Cd for doped and undoped Cu2OSeO3 nanoparticles.

		Cu_2OSeO_3			Cd-Cu_2OSeO_3		
Serial No.	Index peaks/fitting parameters	B.E. (eV)	FWHM (eV)	Area (units)	B.E. (eV)	FWHM (eV)	Area (units)
1	C-1s	284.8	1.1	1.0	284.9	1.2	1.1
2	Cu-$2p_{3/2}$	934.3	2.1	1.9	934.0	2.0	1.7
3	Cu-$2p^*_{3/2}$	934.6	2.4	0.8	943.5	2.1	0.7
4	Cu-$2p1_{/2}$	954.1	1.9	0.9	954.2	2.7	1.2
5	Cu-$2p^*_{1/2}$	962.5	2.4	0.6	962.5	2.2	0.5
6	Se-$3p_{3/2}$	164.7	2.0	1.7	164.8	2.1	1.7
7	Se-$3p_{1/2}$	170.3	1.4	0.3	170.4	1.4	0.3
8	O-1s	530.7	1.5	1.3	530.7	1.5	1.4
9	O-$1s^*$	532.4	2.2	0.7	532.5	2.7	0.6

the bulk state, but also exhibits the phase quality. Despite, the nanocrystals of Cu_2OSeO_3 show the signature of a spin spiral at low temperature below 50 K that can be seen in figures 6(b) and (c). These findings are very significant because our analysis reveals that the present system also lacks the inversion symmetry, ensuring the emergence of DM interaction as in bulk Cu_2OSeO_3. Figures 6(b) and (c) shows the variation of magnetization and its derivative as a function of temperature in the vicinity of skyrmion phase transition. A transition is

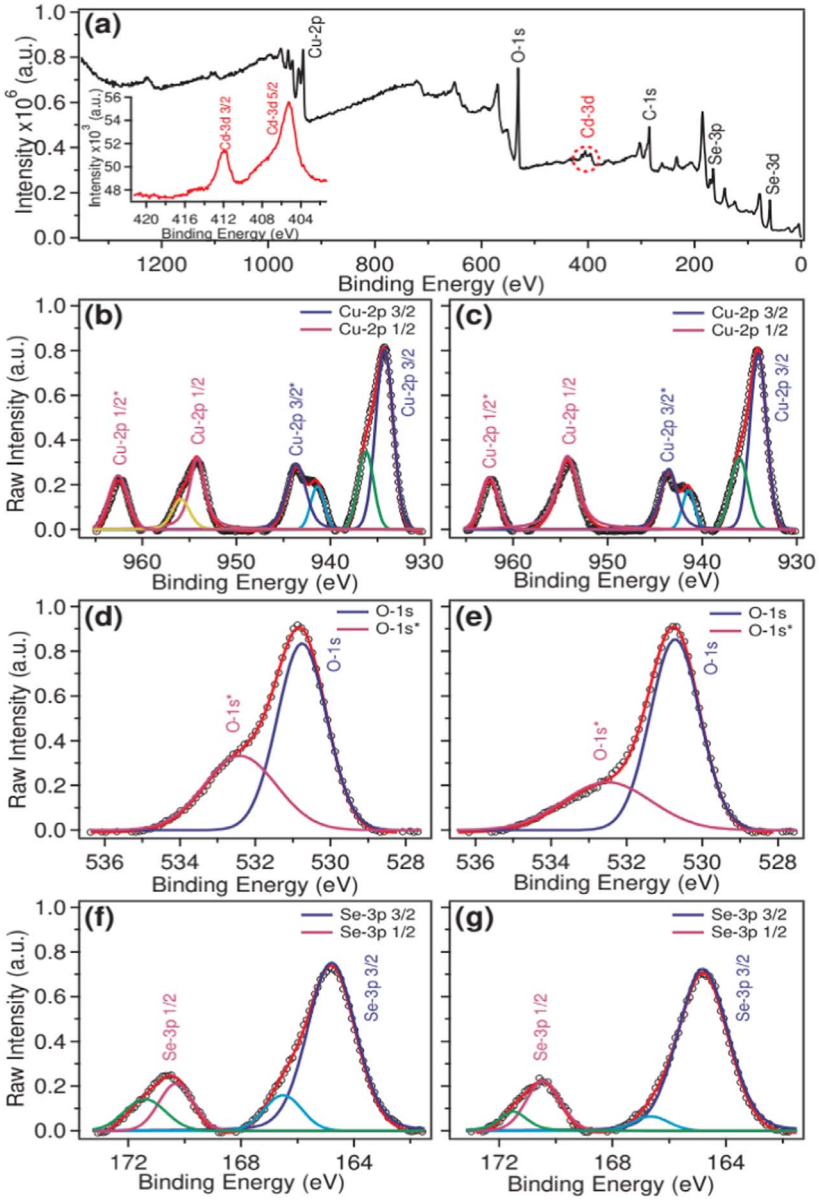

Figure 5. (a) wide- survey XPS scan (b), (c) Cu-2p, (d), (e) O-1s, (f), (g) Se-3p for Cu_2OSeO_3 and $(Cu_{0.98}Cd_{0.02})_2OSeO_3$ nanocrystallites with fitted curves.

appeared at 60 K shown in figure 6(c) for both samples, which is the hallmark signature of materials hosting skyrmion lattice phases [32, 33].

4. Conclusions

In summary, we have demonstrated a strategy for the fabrication of Cu_2OSeO_3 nanocrystallites by solid-state with a nominal Cd (2%) doping followed by one step heat-treatment for 12 h, which is faster than the all the reported route of sample preparation solid-state, hydro-thermal, and chemical route. The XRD patterns reveal Cu_2OSeO_3 phase was stabilized 10 times faster than the conventional solid-state route with a nominal fraction of Cd (2%) followed by one-step heat-treatment for 12 h. TEM data also supports the phase quality and excellent crystallinity of powder sample. The proposed method can result in the elongated Cu_2OSeO_3 nanocrystals (size ~ 50–200 nm) with excellent crystallinity. These findings are essential steps forward the technological applications of magnetic skyrmion for designing the ultra-dense spintronics devices.

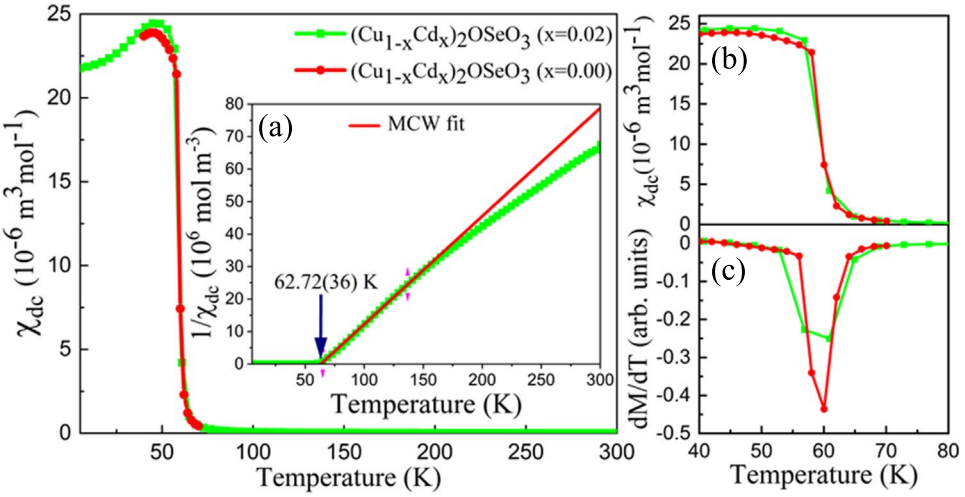

Figure 6. Temperature-dependent magnetization of $(Cu_{0.98}Cd_{0.02})_2OSeO_3$ (x = 0.02) nanocrystals measured in ZFC protocol at 250 Oe. Inset figure (a) represents the $(1/\chi_{dc}, T)$ magnetic susceptibility as a function of temperature. Figure (b) and (c) represent the main magnetic transition and the variation of derivative of magnetization as a function of temperature for doped and undoped samples.

Acknowledgments

Authors would like to acknowledge Central Instrument Facilities, IIT (BHU) for helping with TEM imaging and IIT Delhi for magnetic measurements. This project work is partially financed by DST Nanomission program by project No. IIT (BHU)/R&D/SMST/18-19/09.

ORCID iDs

S Babu https://orcid.org/0000-0002-2892-9175
B K Singh https://orcid.org/0000-0002-4898-8500
S K Mishra https://orcid.org/0000-0001-6140-7443

References

[1] Nagaosa N and Tokura Y 2013 Topological properties and dynamics of magnetic skyrmions *Nat. Nanotechnol.* **8** 899
[2] Rößler U K, Bogdanov A N and Pfleiderer C 2006 Spontaneous skyrmion ground states in magnetic metals *Nature* **442** 797801
[3] Mühlbauer S, Binz B, Jonietz F, Pfleiderer C, Rosch A, Neubauer A, Georgii R and Böni P 2009 Skyrmion lattice in a chiral magnet *Science* **323** 915–91
[4] Fert A, Cros V and Sampaio J 2013 Skyrmions on the track *Nat. Nanotechnol.* **8** 152156
[5] Münzer W *et al* 2010 Skyrmion lattice in the doped semiconductor $Fe_{1-x}Co_xSi$ *Phys. Rev. B* **81** 041203(R)
[6] Wilhelm H, Baenitz M, Schmidt M, Rößler U K, Leonov A A and Bogdanov A N 2011 Precursor phenomena at the magnetic ordering of the cubic helimagnet FeGe *Phys. Rev. Lett.* **107** 127203
[7] Yu X Z, Kanazawa N, Onose Y, Kimoto K, Zhang W Z, Ishiwata S, Matsui Y and Tokura Y 2011 Near room-temperature formation of a skyrmion crystal in thin-films of the helimagnet FeGe *Nat. Mater.* **10** 106109
[8] Janson O, Rousochatzakis I, Tsirlin A A, Belesi M, Leonov A A, Rößler U K, Brink J V D and Rosner H 2014 The quantum nature of skyrmions and half-skyrmions in Cu_2OSeO_3 *Nat.Commun.* **5** 1–11
[9] Du H, DeGrave J P, Xue F, Liang D, Ning W, Yang J, Tian M, Zhang Y and Jin S 2014 Highly stable skyrmion state in helimagnetic MnSi nanowires *Nano Lett.* **14** 2026–32
[10] Chacon A, Heinen L, Halder M, Bauer A, Simeth W, Mühlbauer S, Berger H, Garst M, Rosch A and Pfleiderer C 2018 Observation of two independent skyrmion phases in a chiral magnetic material *Nat. Phys.* **14** 936–41
[11] Karube K *et al* 2016 Robust metastable skyrmions and their triangular square lattice structural transition in a high-temperature chiral magnet *Nat. Mater.* **15** 12371242
[12] Morikawa D, Yu X, Karube K, Tokunaga Y, Taguchi Y, Arima T and Tokura Y 2017 Deformation of topologically- protected supercooled skyrmions in a thin plate of chiral magnet $Co_8Zn_8Mn_4$ *Nano Lett.* **17** 16371641
[13] Oike H, Kikkawa A, Kanazawa N, Taguchi Y, Kawasaki M, Tokura Y and Kagawa F 2016 Interplay between topological and thermodynamic stability in a metastable magnetic skyrmion *Lattice Nat.Phys.* **12** 6266
[14] Kagawa F, Oike H, Koshibae W, Kikkawa A, Okamura Y, Taguchi Y, Nagaosa N and Tokura Y 2017 Current-induced viscoelastic topological unwinding of metastable skyrmion strings *Nat. Commun.* **8** 1332
[15] Okamura Y, Kagawa F, Seki S and Tokura Y 2016 Transition to and from the skyrmion lattice phase by electric fields in a magnetoelectric compound *Nat. Commun.* **7** 12669

[16] Bannenberg L J, Wilhelm H, Cubitt R, Labh A, Schmidt M P, Lelívre-Berna E, Pappas C, Mostovoy M and Leonov A O 2019 Multiple low-temperature skyrmionic states in a bulk chiral magnet *npj Quantum Mater.* **4** 11
[17] Wu H, Wei T, Chandrasekhar K, Chen T, Berger H and Yang H 2015 Unexpected observation of splitting of skyrmion phase in Zn -doped Cu_2OSeO_3 *Sci. Rep.* **5** 13579
[18] Chandrasekhar K D, Wu H, Huang C and Yang H 2016 Effects of Jahn-Teller distortion on the skyrmion stability of (Cu1-xNix)2$OSeO_3$ *J. Mater. Chem. C* **4** 5270–4
[19] Bos J-W G, Colin C V and Palstra T T M 2008 Magnetoelectric coupling in the cubic ferrimagnet Cu_2OSeO_3 *Physical Review B* **78** 094416
[20] Belesi M, Rousochatzakis I, Wu H C, Berger H, Shvets I V, Mila F and Ansermet J P 2010 Ferrimagnetism of the magnetoelectric compound Cu_2OSeO_3 *Physical Review B* **82** 094422
[21] Maisuradze A, Guguchia Z, Graneli B, Rnnow H M, Berger H and Keller H 2011 μSR investigation of magnetism and magnetoelectric coupling in Cu_2OSeO_3 *Physical Review B* **84** 064433
[22] Yang J-H, Li Z-L, Lu X Z, Whangbo M H, Wei S-H, Gong X G and Xiang H J 2012 Strong Dzyaloshinskii-Moriya Interaction and Origin of Ferroelectricity in Cu_2OSeO_3 *Phys. Rev. Lett.* **109** 107203
[23] Zivkovíc I, Pajíc D, Ivek T and Berger H 2012 Two-step transition in a magnetoelectric ferrimagnet Cu_2OSeO_3 *Phys. Rev. B* **85** 224402
[24] Stefancic A *et al* 2015 Origin of skyrmion lattice phase splitting in Zn-substituted Cu_2OSeO_3 *Phys. Rev. Mater.* **2** 111402(R)
[25] Sukhanov A S, Vir P, Cameron A S, Wu H C, Martin N, Mühlbauer S, Heinemann A, Yang H D, Felser C and Inosov D S 2015 Increasing skyrmion stability in Cu_2OSeO_3 by chemical substitution *Phys. Rev. B* **100** 184408
[26] Rodrguez-Carvajal J 2001 Recent developments of the program FullProf *Newsletter of the Commission for Powder Diffraction of the IUCr* **26** 12–9
[27] Cullity B D 1956 *Elements of X Ray Diffraction* (USA: Addison-Wesley Publishing Company, Inc.) p 99 Chap 3
[28] Miloslav K 2017 More features, more tools, more CrysTBox *J. Appl. Cryst.* **50** 12261234
[29] Padmini E and Ramachandran K 2019 Investigation on versatile behaviour of Cd doped $SrTiO_3$ perovskite structured compounds *Solid State Comm.* **302** 113716
[30] Zhang G, Mao C and Wang J 2019 Numerical Analysis and Experimental Studies on the Residual Stress of W/2024Al Composites *Materials* **12** 2746
[31] Manolata M D *et al* 2019 The limit to realize an isolated magnetic single skyrmionic state *J. Mater. Chem. C* **7** 1337
[32] Versteeg R B, Vergara I, Schäfer S D, Bischoff D, Aqeel A, Palstra T T M, Grüninger M and van Loosdrecht P H M 2016 Optically probed symmetry breaking in the chiral magnet Cu_2OSeO_3 *Phys. Rev. B* **94** 094409
[33] White J S *et al* 2014 Electric-Field-Induced Skyrmion Distortion and Giant Lattice Rotation in the Magnetoelectric Insulator Cu_2OSeO_3 *Phys. Rev. Lett.* **113** 107203